Nuclear Instruments and Methods in Physics Research A 664 (2012) 103–110

Contents lists available at SciVerse ScienceDirect

Nuclear Instruments and Methods in Physics Research A

journal homepage: www.elsevier.com/locate/nima

Spatial distribution of thorium fission rate in a fast spallation and fission neutron field: An experimental and Monte Carlo study

J.J. Borger [a], S.R. Hashemi-Nezhad [a,*], D. Alexiev [a], R. Brandt [b], W. Westmeier [b], B. Thomauske [c], J. Adam [d], M. Kadykov [d], S. Tiutiunnikov [d]

[a] School of Physics, University of Sydney, NSW 2006, Australia
[b] Kernchemie Institute, Philipps-Universität, 35032 Marburg, Germany
[c] Forschungzentrum Jülich, ISR-6, 52425 Jülich, Germany
[d] Joint Institute for Nuclear Research, 141980 Dubna, Russian Federation

ARTICLE INFO

Article history:
Received 21 July 2011
Received in revised form
6 October 2011
Accepted 19 October 2011
Available online 7 November 2011

Keywords:
Accelerator-driven Systems
Thorium fission
Neutron-induced fission
Proton-induced fission
Deuteron-induced fission
MCNPX code

ABSTRACT

The Energy plus Transmutation (EpT) set-up of the Joint Institute for Nuclear Research (JINR), Dubna, Russia is composed of a lead spallation target surrounded by a blanket of natural uranium. The resultant neutron spectrum is a combination of spallation and fission spectra, modified by a reflective external layer of polyethylene and an internal absorbing layer of cadmium. The EpT set-up was irradiated with a beam of 4 GeV deuterons from the Nuclotron Accelerator at JINR. The spatial distribution of thorium fission rate within the assembly was determined experimentally, using a fission track detector technique, and compared with Monte Carlo predictions of the MCNPX code. Contributions of neutrons, protons, deuterons, photons and pions to total fission were taken into account. Close agreement between the experimental and calculated results was found.

© 2011 Elsevier B.V. All rights reserved.

1. Introduction

1.1. Accelerator driven systems

Accelerator driven systems (ADS) are sub-critical reactors which rely on a spallation neutron source to maintain fission chain reactions [1,2]. The ideal target is normally considered to be a heavy metal such as lead (see e.g. Ref. [3]) but, recently, it has been shown that there are significant gains in efficiency to be obtained from using uranium targets and deuteron beams [4]. The neutron spectrum of an ADS is expected to be a combination of a spallation neutron spectrum stretching up to the energy of the incident ions (in the range of GeV), and a fission neutron spectrum (see, for example, Fig. 3a). Thorium (^{232}Th) is mooted as a suitable fertile material from which the fuel (^{233}U) is bred through neutron absorption and subsequent beta decays. Despite the fact that the bulk of the energy of the system is to be produced from fission of ^{233}U, ^{232}Th also possesses a significant fission cross-section for fast neutrons (see Fig. 4). Therefore, significant energy production can be expected from fission of ^{232}Th, and its fission rates in ADS spectra are of great interest in future ADS designs.

1.2. The energy plus transmutation set-up

The Energy plus Transmutation (EpT) set-up (Fig. 1) is designed to emulate the neutron spectrum expected in a fast ADS. It consists of a spallation target of natural lead surrounded by a blanket of natural uranium rods (total mass of natural uranium is 206.4 kg). The target and blanket are divided into four equal-length sections with gaps of 8 mm between them. Samples may be mounted on sample plates and placed in these gaps and at the front and back of the target–blanket. These positions are labelled 1–5 in Fig. 1b. In this way the combined spallation and fission spectrum can be studied. The target and blanket itself is surrounded by neutron reflecting shielding consisting of granulated polyethylene. On the interior surfaces of this shielding is a 1 mm thick layer of cadmium (also indicated in Fig. 1) to prevent thermal neutrons from entering the blanket region. More detailed descriptions of the EpT set-up are available elsewhere [5,6].

1.3. The fission track detector technique

In the fission track detector technique, a foil of fissionable material is sandwiched between wafers of an appropriate solid state nuclear track detector (SSNTD). In the present paper the SSNTD used is synthetic fluorophlogopite mica. Fission events close to the surface of the fission foil can result in the ejection of

* Corresponding author. Tel.: +61 2 9351 5964.
E-mail address: reza@physics.usyd.edu.au (S.R. Hashemi-Nezhad).

0168-9002/$ - see front matter © 2011 Elsevier B.V. All rights reserved.
doi:10.1016/j.nima.2011.10.027

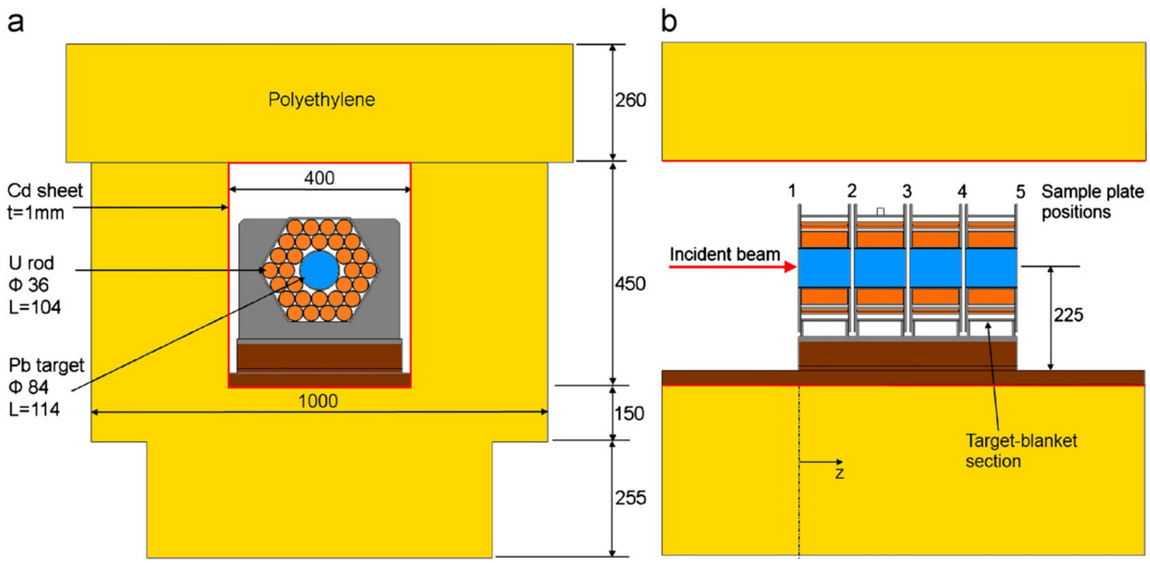

Fig. 1. Layout of EpT set-up, showing the central lead target, blanket of natural uranium rods and surrounding polyethylene shielding (all dimensions given in mm). (a) *X–Y* cross-section, (b) *Y–Z* cross-section. Lengths of U rod and Pb target are for one target-blanket section only.

fission fragments which record etch-able tracks in the mica. Mica is the preferred SSNTD material for this type of measurement since it has the advantage of being insensitive to α particles which are emitted by many fissionable isotopes.

In order to measure fission rate, a calibration factor is required to relate the density of tracks in the mica to the number of fissions occurring in the foil material. Earlier work [7] discussed the calibration process in detail and provided calibration factors for ^{nat}U and ^{235}U fission. These results were used to determine the fission rate of uranium in the EpT set-up under 1.5 GeV proton irradiation [5]. Recently, calibrations have been carried out for fission of ^{nat}Pb, ^{197}Au and ^{232}Th [8].

The fission rate is related to the track density in the detector by

$$\rho = wN_f \tag{1}$$

where ρ is the mean track density of the forward and backward mica detectors (in tracks cm^{-2}) and N_f is the number of fissions occurring in the foil (per fissionable nucleus in the foil material). In this work a calibration factor of $w = (8.97 \pm 0.23) \times 10^{18}$ tracks cm^{-2} (fissions per atom)$^{-1}$ was used for the thick thorium foils in contact with synthetic mica. This is a weighted mean value obtained from the theoretical and Monte Carlo calculations carried out by Hashemi-Nezhad et al. [8].

2. Experimental

2.1. Sample preparation

Thirty samples were prepared, each comprised a ~50 μm thick and 10 mm diameter metallic thorium foil sandwiched by two ~50 μm thick mica wafers (as shown in Fig. 2a). Since the range of typical fission fragments in thorium is less than 10 μm [8], the foils are considered "thick". Six samples were mounted flat to each of the five sample plates. The plates were mounted at the front and rear of the target/blanket (positions 1 and 5 in Fig. 1b) and in the three gaps between the separate sections of the target/blanket (positions 2–4 in Fig. 1b). On each plate the samples were spaced along a radius rotated 30° to the right from the vertical (as seen by the incident beam), at distances of $r = 0, 3, 6, 8.5, 11$ and 13.5 cm from the target axis (see Fig. 2b).

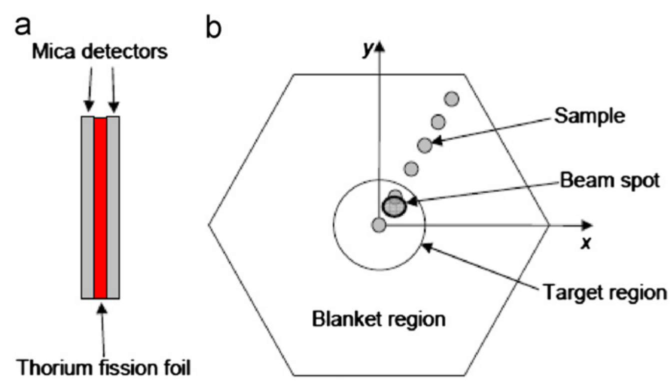

Fig. 2. (a) Cross-section of a foil-mica detector sandwich. (b) Arrangement of sandwich samples, in the *x–y* plane, on each of the sample plates. The samples are shown superimposed with the EpT target–blanket geometry and the measured beam position and shape.

2.2. Irradiation

The spallation target of the EpT set-up was irradiated with a pulsed beam of 4 GeV deuterons from the Nuclotron accelerator at the Joint Institute for Nuclear Research over a period of some 18 h. Further details of the irradiation can be seen in Table 1.

2.2.1. Beam position measurement

The beam position was measured by two separate techniques. One of these used an array of fission detectors measuring beam induced ^{nat}Pb(d,f) reactions [9]. The other measured the activity induced by beam deuterons in a sample of natural copper [10]. Both the fission detector array and the copper sample were mounted directly to the front of the EpT set-up. Both measurements, in agreement to within 1 mm, showed that the beam position lay some distance away from the axis of the target. The mean position and FWHM of the beam are presented in Table 1 and visible in Fig. 2.

2.2.2. Beam fluence measurement

The total deuteron beam fluence was determined with the use of activation of aluminium foils via ^{27}Al(d,x)^{24}Na reactions. Two

Table 1
Irradiation detail.

Location	Nuclotron accelerator, Joint Institute for Nuclear Research
Date	25–26 November 2009
Incident particle	4 GeV deuteron
Irradiation time	18 h (pulsed)
Total fluence	$(1.59 \pm 0.31) \times 10^{13}$ [a]
X co-ordinate of beam	2.4 cm right from centre (FWHM 2.1 cm) [b]
Y co-ordinate of beam	1.7 cm up from centre (FWHM 1.8 cm) [b]

[a] See text for details.
[b] As shown in Fig. 2b.

Table 2
Track densities of samples on plate 2.

Sample position *r* (cm)	Track density (tracks cm^{-2})
0	$(8.10 \pm 0.17) \times 10^6$
3	$(1.11 \pm 0.02) \times 10^7$
6	$(4.39 \pm 0.11) \times 10^6$
8.5	$(2.14 \pm 0.06) \times 10^6$
11	$(1.28 \pm 0.04) \times 10^6$
13.5	$(7.91 \pm 0.31) \times 10^5$

independent but simultaneous measurements were made yielding measured fluences of $(1.99 \pm 0.25) \times 10^{13}$ [10] and $(1.37 \pm 0.19) \times 10^{13}$ [11] deuterons, respectively. The reason for the significant difference between these measurements (approximately 44%) is not clear to the authors. However, it is noted that both measurements are separated by less than 2σ. In the absence of further information it is sensible to treat them as equally valid. Therefore, a weighted mean fluence of $(1.59 \pm 0.31) \times 10^{13}$ deuterons was determined.

2.3. Mica detector processing

After the irradiation all thorium foils were separated from the mica wafers and the wafers were etched for 5–8 min in 7% hydrofluoric acid at 60 °C. Etching time was varied according to balance the need to limit track overlap in samples whose track density was expected to be high, and enhancing development in samples where track density was expected to be low. Track density was determined by counting tracks from sets of images taken from samples using an Olympus CX-41 Microscope coupled to an adapted Nikon D700 digital SLR camera. The recorded track densities in samples on plate 2 are shown in Table 2.

3. Monte Carlo calculations

The MCNPX 2.5.0 code [12] was used to model the EpT set-up (with the same layout as shown in Fig. 1) and all relevant samples. The model was "irradiated" with a 4 GeV beam of deuterons, parallel to the target axis, and with the same shape and position as presented in Table 1. An elliptical beam acceptance region, or "cookie cutter", was defined with a width equal to two full widths at half maximum of the true beam in the *X* and *Y* axes. Given the position and FWHM data for this experiment it is clear that a small proportion of the incident deuterons will not hit the spallation target but instead interact within the uranium blanket or pass through the gaps between the uranium rods. The following options were used in the MCNPX run:

1. Deuterons, neutrons, protons, photons and pions were all transported. Electrons were not transported as this slows down the simulation dramatically without significantly affecting the results.
2. The INCL4 intra-nuclear cascade model [13] was used along with the ABLA fission-evaporation model [14]. Previous calculations have shown that this selection of models provides the best match with experimental data compared to other models [5].
3. The la150n (neutron) and la150h (proton) libraries [15] were used wherever possible. However, many materials present in the model do not have corresponding data in these libraries. In these cases the recently developed ADS-2.0 nuclear data library [16], based upon ENDF/B-VII.0 evaluated data [17], was used. In rare cases where neither la150 nor ADS-2.0 libraries contained the required data, ENDF/B-VI libraries were used instead.
4. The FCL:n=1 (forced neutron collisions) variance reduction option was selected to improve the speed of convergence of the simulation.

3.1. Particle spectra

Fig. 3 shows typical calculated neutron, photon, proton and deuteron spectra experienced by samples placed in the target region and blanket region on sample plate 2 of the EpT set-up (see Fig. 1). The neutrons resulting from spallation in the target and fission in the blanket are slowed down in the surrounding polyethylene shielding. The average spectrum in the shielding (Fig. 3b) indicates significant thermal and epithermal components. Neutrons are also reflected back from the shielding towards the blanket, increasing the number of neutrons relevant to resonance absorption. However, the 1 mm thick cadmium layer on the internal surfaces of the polyethylene shielding (also shown in Fig. 1) prevents the reflection of thermal neutrons. This effect is clearly visible in comparison of the shapes of the spectra in Fig. 3a and b in the region below about 1 eV. Thus the fast, resonance and epithermal regions of the neutron spectrum can be investigated with samples placed in the target and blanket regions whilst thermal neutrons may be studied by the placement of samples inside or on the exterior of the polyethylene shielding.

It is clear from Fig. 3a that samples further from the beam axis are subject to progressively softer neutron spectra. Whilst those nearer to the beam axis are subjected to far more neutrons resulting from spallation reactions in the target.

Protons (Fig. 3d) are mainly emitted in the course of spallation reactions in the target as well as other nuclear reactions in the target and blanket.

A peak is visible in the proton and neutron spectra in the target region at about 2 GeV (half the incident deuteron energy) in Fig. 3a and d. However, both these peaks exhibit a high energy tail. The incident deuteron consists of a loosely bound proton and neutron, and can break up through Coulomb interactions [18], scattering events [19,20] and in the course of direct reactions [21]. The energy sharing between the proton and neutron resulting from such a break-up is not necessarily equal [18,22,13], leading to the production of neutrons and protons at energies higher than half the incident deuteron energy. The presence of these peaks, and their associated high energy tails in the simulated spectra of Fig. 3 indicates that these mechanisms are included in the INCL4 model [13] used in our simulations.

The deuteron spectrum in the target region (Fig. 3d) shows the prominent peak at 4 GeV, indicating that the majority of deuterons in this region are incident beam deuterons. Small numbers of deuterons also result from spallation and other reactions and these are visible at energies below about 150 MeV.

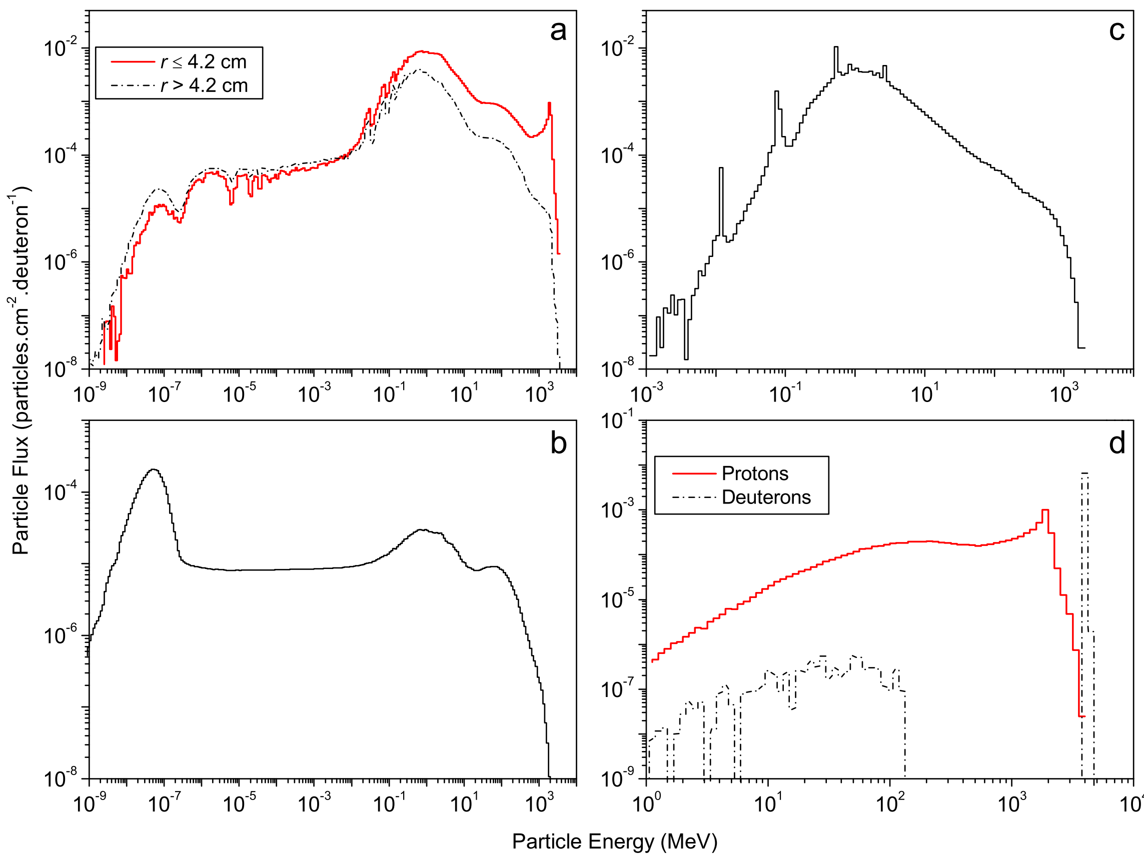

Fig. 3. Simulated particle spectra in the gap for plate 2, between the first and second target–blanket sections of the EpT set-up (see Fig. 1b): (a) Neutron spectra in the target ($r \leq 4.2$ cm) and blanket ($r > 4.2$ cm) regions. The effect of the cadmium sheet (also shown in Fig. 1) on the neutrons reflected back into the target and blanket regions is clearly visible below ~ 1 eV. (b) Average neutron spectrum in the polyethylene shielding (surrounding the target and blanket in Fig. 1). (c) Photon spectrum in the target region. (d) Proton and deuteron spectra in the target region. *Note that scales are not the same for all plots.*

The photon spectrum in the target region (Fig. 3c) indicates a broad continuum extending to 2 GeV. Also visible are the characteristic X-ray peaks of lead at ~ 80 keV (K-series) and ~ 11 keV (L-series).

3.2. Cross-sections for thorium fission

Samples in the set-up are subject to fission induced by neutrons, protons, deuterons and photons, depending on sample location. Fission in the blanket region (6–13.5 cm from the target axis) is due mainly to (n,f) reactions, whilst fission nearer the target axis is due to (n,f), (p,f) and (d,f) reactions. All samples would also be subjected to a certain level of (γ,f) reactions.

3.2.1. Neutron-induced fission cross-section

In the case of thorium, no la150n library is available. Therefore, use was made of the ADS Lib 2.0 data library [16], in which the cross-section evaluation for ^{232}Th(n,f) has a maximum incident neutron energy of 60 MeV. The cross-section data of Shcherbakov et al. [23] were used for neutrons between 60 MeV and 200 MeV. For neutrons above 200 MeV the data of Paradela et al. [24] was used. These points (extending to almost 980 MeV) were fitted with a second order polynomial and then normalised to Shcherbakov's data at 200 MeV. The data used for the ^{232}Th(n,f) cross-section are shown in Fig. 4.

Above 980 MeV, no experimental or modelled data could be found, so the cross-section at 980 MeV was extrapolated for neutrons of higher energy. In this region the fission cross-section is expected to scale with the geometric cross-section (i.e. remaining approximately constant). Sample plate 2 (see Fig. 1b) is the plate with the highest neutron fluxes and reaction rates. It is noted that the flux of neutrons above 1 GeV in samples in this position is 3% of total neutron flux in the target region ($r \leq 4.2$ cm) and 0.3% of total neutron flux in the blanket region ($r > 4.2$ cm) (see Fig. 3a). Any error introduced by the assumption of constant (n,f) cross-section above 980 MeV is therefore small.

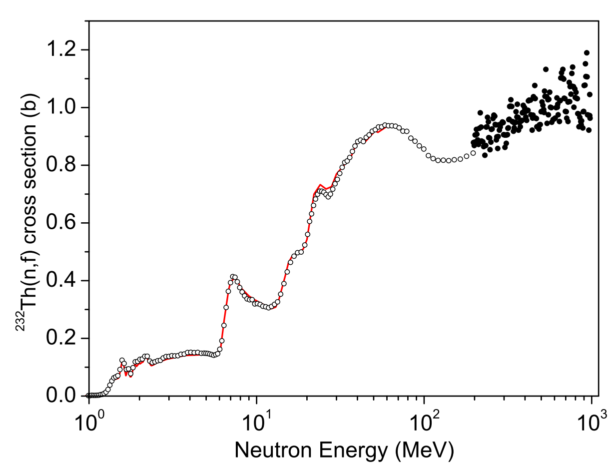

Fig. 4. ^{232}Th(n,f) cross-section as a function of incident neutron energy. The solid line represents data from the ENDF/B-VII.0 evaluation (up to 60 MeV); open circles represent the data of Shcherbakov et al. [23]; and filled circles represent the data of Paradela et al. [24] above 200 MeV.

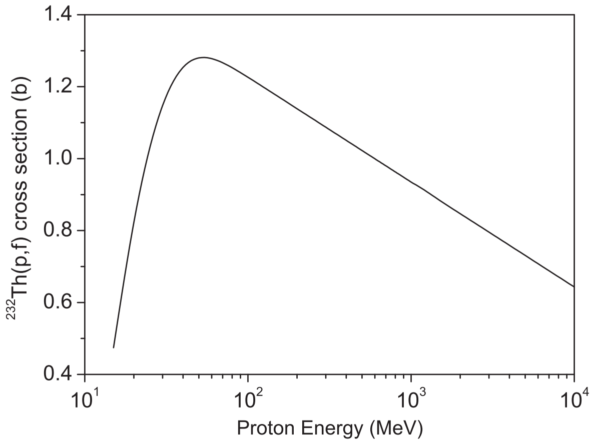

Fig. 5. ^{232}Th(p,f) cross-section as a function of incident proton energy, obtained from parameterisation [25].

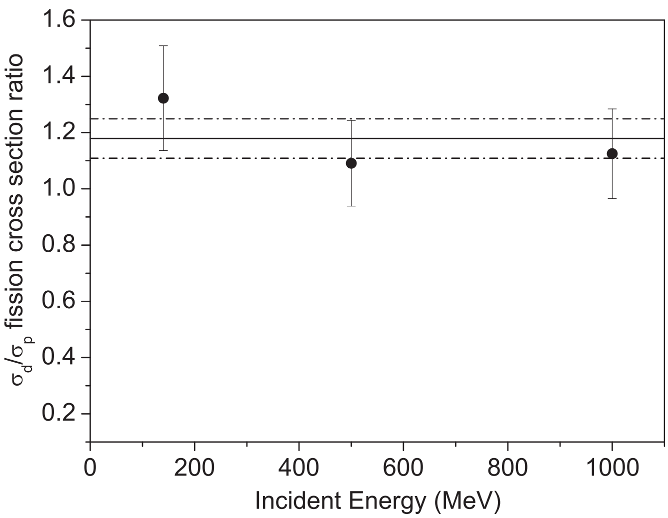

Fig. 6. Ratio of ^{232}Th(d,f) cross-section to the ^{232}Th(p,f) cross-section (σ_d/σ_p) as determined from experimental data of Saint-Laurent et al. [26] (filled circles). Lines represent the mean and SEM values of σ_d/σ_p.

3.2.2. Proton-, deuteron- and photon-induced fission cross-sections

The ^{232}Th(p,f) cross-section data were obtained from a best fit parameterisation of available experimental data, as described by Prokofiev [25] (see Fig. 5).

For deuterons no such parameterisation exists. However, one set of measurements for both ^{232}Th(p,f) and ^{232}Th(d,f) cross-sections at corresponding energies of 140, 500 and 1000 MeV is available [26]. From these measurements the ratio of (d,f) to (p,f) cross-section, σ_d/σ_p was calculated (plotted in Fig. 6). The value of σ_d/σ_p appears constant, within experimental uncertainty, over a broad range of incident energies. The mean value of σ_d/σ_p was found to be 1.18 ± 0.07. This value was used as a scaling factor to provide an estimate of the ^{232}Th(d,f) cross-section from the parameterised (p,f) cross-section. The vast majority of deuterons in the system are due to the incident 4 GeV beam and therefore any error introduced by this method of cross-section estimation is expected to be confined to samples lying in the beam.

The (γ,f) (photofission) cross-section values were obtained from available experimental data [27–29]. These are shown in Fig. 7. Linear interpolation in log scale was used to obtain the cross-section values used in the Monte Carlo calculations.

Pion induced fission is also possible. However, a previous study, using the same set-up to measure the uranium fission rate, found that the rate of the (π,f) reactions in the EpT blanket

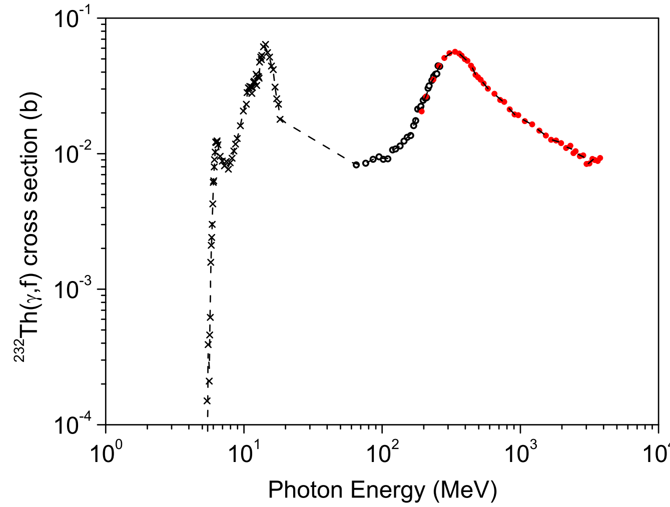

Fig. 7. ^{232}Th(γ,f) cross-section as a function of photon energy. Crosses represent the data of Caldwell et al. [27], open circles represent the data of Sanabria et al. [28], and filled circles represent the data of Cetina et al. [29]. Linear interpolation on log scale was used (dashed line).

region amounted to only 0.4% of the total ^{nat}U fission rate [5]. This rate lies well within the margin of experimental uncertainty in that study. The ^{232}Th(π^+,f) cross-section has been measured to be 1.8 b at 80 MeV [30] whilst the same cross-section for ^{nat}U was found to be 2.02 b [31]. Given, then, that the rate of (π,f) reactions can only be lower in the ^{232}Th samples than in ^{nat}U, the effect of pion induced fission is not expected to be significant in the present study.

4. Results

Fig. 8 shows the comparison between the measured fission rates from the EpT set-up and those determined from Monte Carlo calculations. All data are presented in terms of a B-value (reactions per gramme of sample per incident deuteron). Agreement is found within $\pm 2\sigma$ for samples which do not lie in the path of the direct beam. As expected, the contribution of deuterons to fission in these samples is never more than 1%. There is significant disagreement, however, for samples at $r = 3$ cm which lie partly in the deuteron beam. For this sample on plate 1 Monte Carlo estimates 2.43 times higher fission rate compared with the measured rate. This factor decreases to 1.82 for the sample on plate 2 and continues to decrease further until the measured and calculated rates are in agreement at $r = 3$ cm on plate 5. This is a clear indication that the discrepancy is related to ^{232}Th(d,f) interactions as the deuteron intensity decreases for samples away from the target region (as r increases), and for samples further from the point of beam entry (as z increases towards plate 5). The possible causes of this behaviour are discussed below.

4.1. The effect of beam position

The beam position measurements (Table 1) indicate that the samples placed at $r = 3$ cm lie in a position within one FWHM of the beam centre co-ordinates (see Fig. 2b). In these samples, the rate of fission due to deuterons is not uniform and the fission track density in these samples will vary significantly across the area of the sample. Initial values of track density were obtained from taking a few images in the centre of the sample. Therefore, several of the samples placed at $r = 3$ cm were recounted by taking images in a prescribed pattern across the mica to ensure a

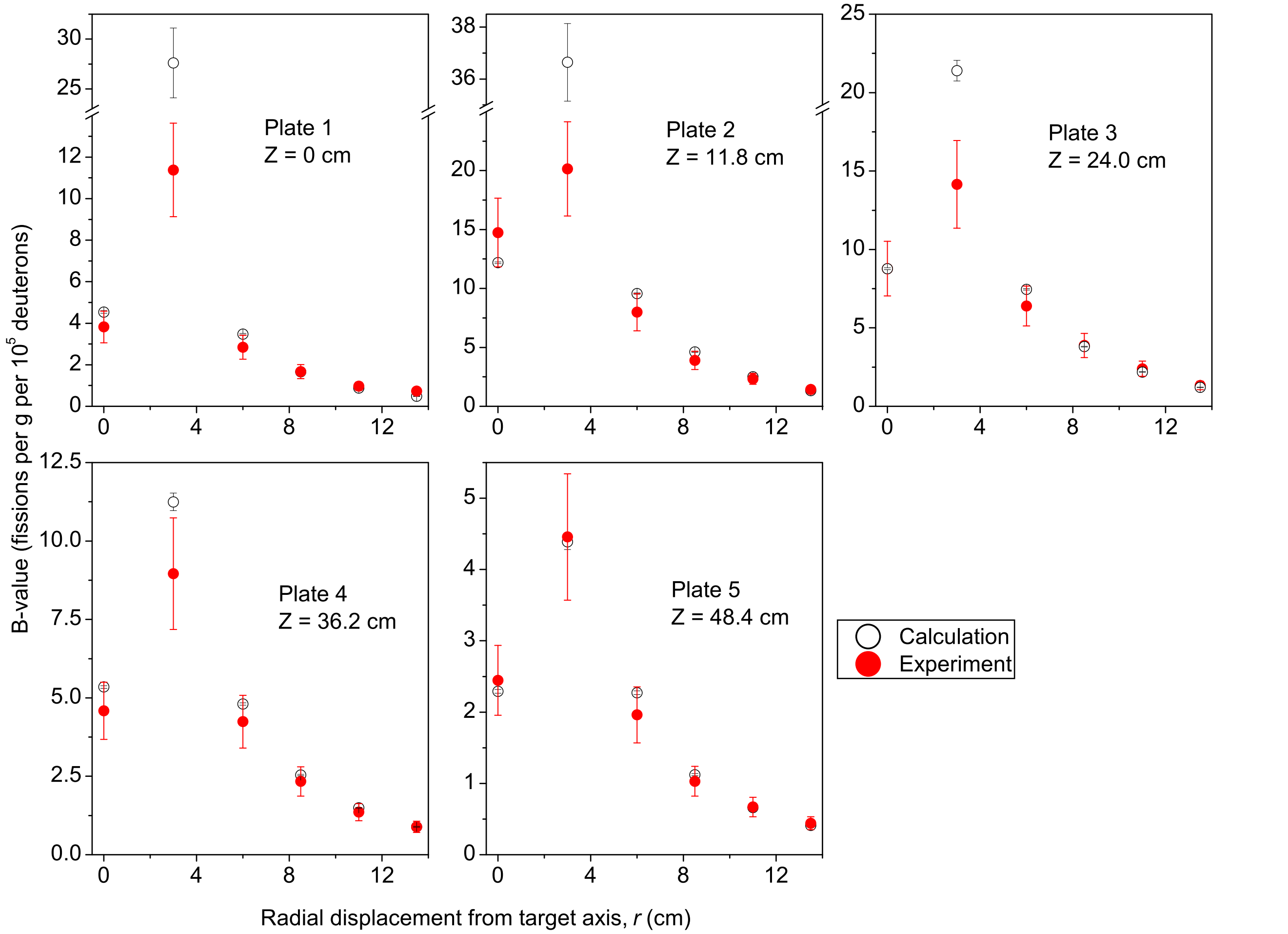

Fig. 8. Radial variation of the total ^{232}Th fission rate due to neutrons, protons, deuterons and photons. Data for plates 1 and 2 have broken axes to avoid the compression of data points for $r>4$ cm. *Note that vertical scales are not the same for all plots.*

more complete sampling of the variation in track density across the sample. The mean track density obtained using this method, however, was found to differ from the original count by less than 2% (within experimental uncertainty).

The samples placed in the set-up (including the samples used to measure beam position) were mounted on acetate sheets which were aligned to the axis of the spallation target by hand. This introduces an uncertainty in the measured beam centre co-ordinates (X_c,Y_c) with respect to the target axis and with respect to the fission foils.

To study the effect of variation of the beam centre co-ordinates on the calculated fission rates and their spatial distribution, several Monte Carlo calculations were made with the beam position shifted by amounts $\pm\Delta X_c$ and $\pm\Delta Y_c$ from the measured position. Given the magnitudes of FWHM in X and Y axes for the beam shape in Table 1, and the method used to mount and align the samples, we consider shifts of $\Delta X_c=\Delta Y_c=0.5$ cm to provide a conservative estimate of this uncertainty.

Fig. 9 shows the effect of vertical ($\Delta Y_c=0.5$ cm) beam shifts on the fission rates in samples on plate 2. The effect is most pronounced in the samples closest to the beam axis (at $r=3$ cm). In the sample at this position on plate 2, a 0.5 cm beam position uncertainty results in the introduction of a ± 29% uncertainty in the fission rate. For a sample with the same r on plate 1 the resulting introduced uncertainty is ± 44%. Some introduced uncertainty is also clear in samples at $r=0$ cm and 6 cm (± 20% and ± 10%, respectively, on plate 2).

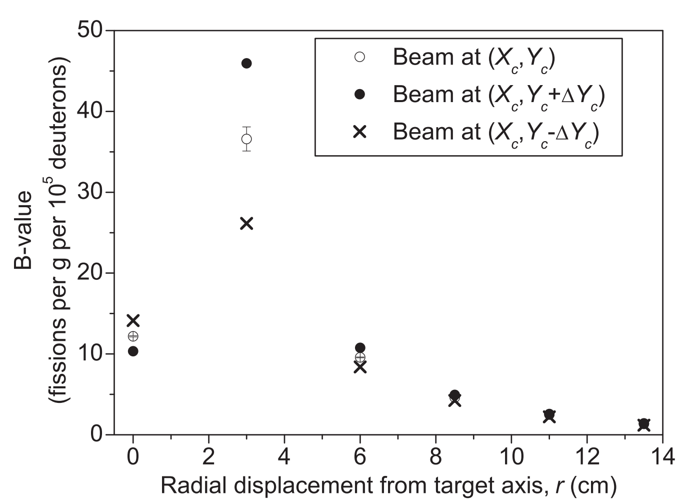

Fig. 9. Total ^{232}Th fission in plate 2, determined by Monte Carlo calculations, for deuteron beams at the measured position, (X_c,Y_c) and at positions (X_c, $Y_c\pm\Delta Y_c$), with $\Delta Y_c=0.5$ cm.

The results of this investigation are incorporated into the uncertainty of the results presented in Fig. 10. Here it is clear that if the uncertainty in relative beam-sample position is included, agreement within $\pm 1\sigma$ is found for all samples, apart from that at $r=3$ cm on plate 2, where agreement better than $\pm 2\sigma$ is found.

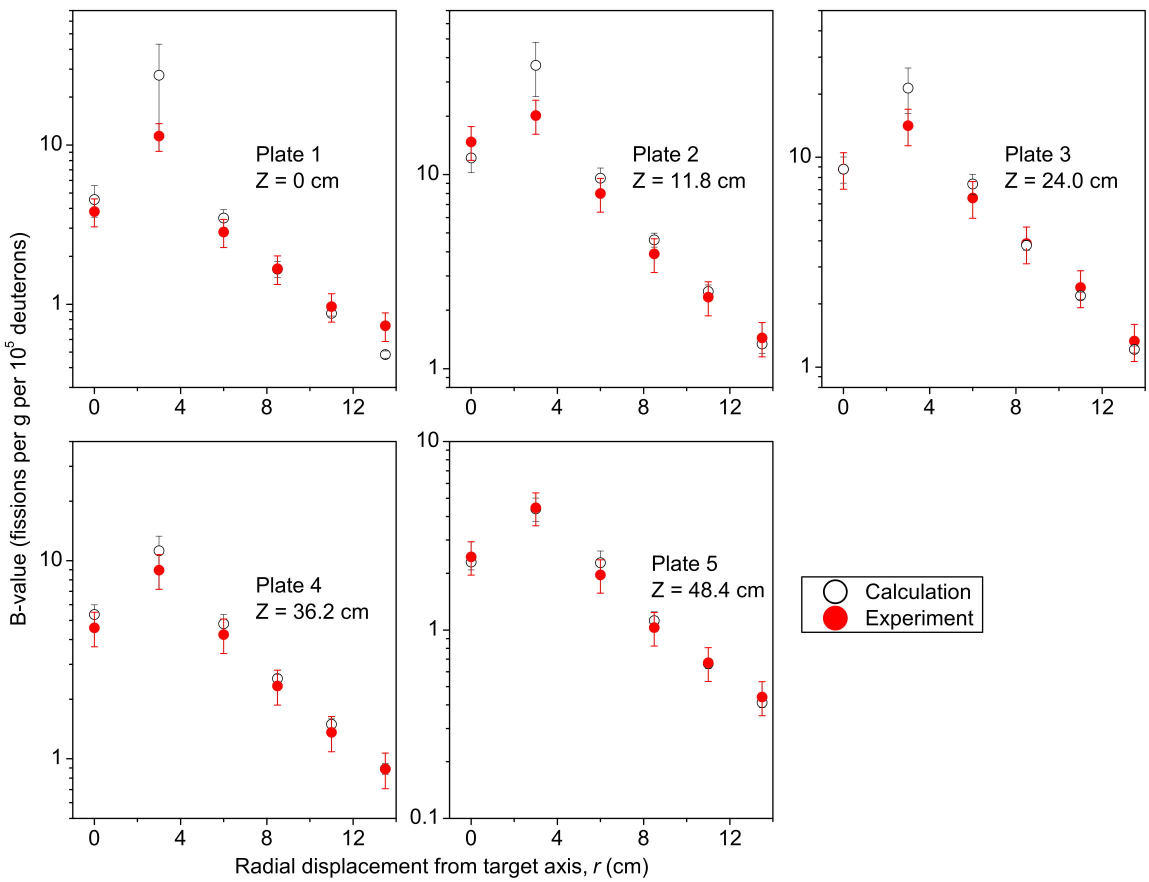

Fig. 10. Radial variation of the total ^{232}Th fission rate in plates 1–5 including the effect of beam position uncertainty (cf. Fig. 8). Data are presented on logarithmic vertical scales. *Note that the vertical scales are not the same for all plots.*

4.2. Cross-sections for proton and deuteron induced fission

The parameterisation used for the variation of the ^{232}Th(p,f) cross-section with energy depends heavily on the reliability of the included experimental measurements. However, as stated by Prokofiev [25], many of the experimental data for the ^{232}Th(p,f) cross-section are discrepant and, in some cases, contradictory in the energy region above 1 GeV. Moreover the cross-section parameterisation appears to carry significant uncertainty (with respect to experimental data) in the energy region above 100 MeV. The ^{232}Th(p,f) parameterisation was determined by Prokofiev to be the one in most need of further experimental study [25].

The fact that very little data exists for deuteron induced fission has necessitated that this parameterisation also be used for the (d,f) cross-section (scaled by the factor σ_d/σ_p). Therefore, any error in the parameterisation for the ^{232}Th(p,f) cross-section is also present in the ^{232}Th(d,f) cross-section.

As seen from our results, fuel placed near to the spallation target of future ADS will be subject to significant levels of charged particle induced fission. We therefore echo Prokofiev's sentiment that more experimental work in this area is needed for future ADS development.

5. Conclusion

The spatial distribution of thorium fission rate in a combined spallation and fission neutron field was determined using the Energy plus Transmutation experimental set-up combined with the fission track detector technique. Comparison was made between the results of these measurements and results from Monte Carlo simulations using the MCNPX 2.5.0 code. When the uncertainty in beam position, relative to sample positions, was taken into account, results were found to be in $\pm 1\sigma$ agreement for samples which did not lie in the path of the incident beam, and within $\pm 2\sigma$ agreement for samples which lay in the path of the incident beam.

The proton- and deuteron-induced fission rates (determined through the use of parameterised cross-sections) appear to be overestimated. It is expected that this effect is largely due to the fact that the currently available experimental data include many discrepant cross-section values [25]. Further experimental studies on proton induced fission of ^{232}Th are needed to clarify this. The obvious sparseness of deuteron induced fission data is also an area of urgent need for ADS development; particularly since spallation neutron production efficiency is maximised by use of incident deuteron beams [4].

Despite this, the fast neutron distribution in the blanket region seems well described by the codes used. This region is analogous to the fuel region of an accelerator driven system, so it is expected that the spatial distribution of thorium fission in the fuel regions of ADS would also be well described by the same code system.

Acknowledgements

We would like to express our gratitude to the Veksler and Baldin Laboratory of High Energies and the staff of the Nuclotron accelerator for providing the research facilities used in these experiments. Some of us are also indebted to the Joint Institute for Nuclear Research for their generous hospitality during our stay in Dubna.

References

[1] C. Bowman, E. Arthur, P. Lisowski, G. Lawrence, R. Jensen, J. Anderson, B. Blind, M. Cappiello, J. Davidson, T. England, L. Engel, R. Haight, H.G. Hughes III, J. Ireland, R. Krakowski, R. LaBauve, B. Letellier, R. Perry, G. Russell, K. Staudhammer, G. Versamis, W.B. Wilson, Nuclear Instruments and Methods in Physics Research Section A 320 (1992) 336.

[2] F. Carminati, R. Klapisch, J.P. Revol, C. Roche, A. Rubio, C. Rubbia, An Energy Amplifier for Cleaner and Inexhaustible Nuclear Energy Production Driven by a Particle Beam Accelerator, Technical Report, CERN-AT-93-47-ET, CERN, 1993.

[3] S.R. Hashemi-Nezhad, R. Brandt, W. Westmeier, V.P. Bamblevski, M.I. Krivopustov, B.A. Kulakov, A.N. Sosnin, J.-S. Wan, R. Odoj, Kerntechnik 66 (2001) 1.

[4] S.R. Hashemi-Nezhad, W. Westmeier, M. Zamani-Valasiadou, B. Thomauske, R. Brandt, Annals of Nuclear Energy 38 (5) (2011) 1144.

[5] S.R. Hashemi-Nezhad, I. Zhuk, M. Kievets, M. Krivopustov, A. Sosnin, W. Westmeier, R. Brandt, Nuclear Instruments and Methods in Physics Research Section A 591 (2008) 517.

[6] M. Krivopustov, A. Pavliouk, A. Kovalenko, I. Mariin, A. Elishev, J. Adam, A. Kovalik, Y. Batusov, V. Kalinnikov, V. Brudanin, P. Chaloun, V. Tsoupko-Sitnikov, A. Solnyshkin, V. Stegailov, S. Gerbish, O. Svoboda, Z. Dubnicka, M. Kala, M. Kloc, A. Krasa, A. Kugler, M. Majerle, V. Wagner, R. Brandt, W. Westmeier, H. Robotham, K. Siemon, M. Bielewicz, S. Kilim, M. Szuta, E. Strugalska-Gola, A. Wojeciechowski, S.R. Hashemi-Nezhad, M. Manolopoulou, M. Fragopolou, S. Stoulos, M. Zamani-Valasiadou, S. Jokic, K. Katovsky, O. Schastny, I. Zhuk, A. Potapenko, A. Safronova, Z. Lukashevich, V. Voronko, V. Sotnikov, V. Sidorenko, W. Ensinger, H. Severin, S. Batsev, L. Kostov, K. Protokhristov, C. Stoyanov, O. Yordanov, P. Zhivkov, A. Kumar, M. Sharma, A. Khilmanovich, B. Marcinkevich, S. Korneev, T. Damdinsuren, T. Togoo, H. Kumawat, Journal of Radioanalytical and Nuclear Chemistry 279 (2) (2009) 567.

[7] S.R. Hashemi-Nezhad, I.V. Zhuk, A.S. Potapenko, M. Krivopustov, Nuclear Instruments and Methods in Physics Research Section A 568 (2006) 816.

[8] S.R. Hashemi-Nezhad, I.V. Zhuk, A.S. Potapenko, M.K. Kievets, M. Krivopustov, Nuclear Instruments and Methods in Physics Research Section A, doi: 10.1016/j.nima.2011.10.029, in press.

[9] A.S. Potapenko, A.A. Safronova, I.V. Zhuk, V.A. Voronko, V.V. Sotnikov, P.A. Martynenko, Yu.T. Petrusenko, Methods and results of the ^{nat}Pb(d,f), ^{209}Bi(d,f) and ^{209}Bi(d,xnyp) reactions cross-sections measurements at 1.6 and 4 GeV deuteron beams, in: ISHEPP XX—International Baldin Seminar on High Energy Physics Problems: Relativistic Nuclear Physics And Quantum Chromodynamics, Dubna, Russia, October 2010.

[10] O. Svoboda, V. Wagner, D. Wagner, The Intensity and Shape of the 4 GeV Deuteron Beam from the JINR Nuclotron (November 2009)—Results from the Řež Group, 2010.

[11] W. Westmeier, Experiment S: 4.00 GeV Deuterons on E + T, Technical Report, Du-Ma Collaboration, 2011.

[12] D.P. Pelowitz, MCNPX User's Manual: Version 2.5.0, Technical Report, LA-CP-05-0369, Los Alamos National Laboratory and University of California, April 2005.

[13] A. Boudard, J. Cugnon, S. Leray, C. Volant, Physical Review C 66 (2002) 044615.

[14] J.J. Gaimard, K.H. Schmidt, Nuclear Physics A 531 (1991) 709.

[15] M.B. Chadwick, P.G. Young, S. Chiba, S.C. Frankle, G.M. Hale, H.G. Hugher, A.J. Koning, R.C. Little, R.E. MacFarlane, R.E. Prael, L.S. Waters, Nuclear Science and Engineering 131 (1999) 293.

[16] D. Lopez Aldama, A.L. Nichols, ADS-2.0 A Test Library for Accelerator Driven Systems and New Reactor Designs, Technical Report, INDC(NDS)-0545, International Atomic Energy Agency, Vienna, 2008.

[17] M.B. Chadwick, P. Oblozinsky, M. Herman, N.M. Greene, R.D. McKnight, D.L. Smith, P.G. Young, R.E. MacFarlane, G.M. Hale, S.C. Frankle, A.C. Kahler, T. Kawano, R.C. Little, D.G. Madland, P. Moller, R.D. Mosteller, P.R. Page, P. Talou, H. Trellue, M.C. White, W.B. Wilson, R. Arcilla, C.L. Dunford, S.F. Mughabghab, B. Pritychenko, D. Rochman, A.A. Sonzogni, C.R. Lubitz, T.H. Trumbull, J.P. Weinman, D.A. Brown, D.E. Cullen, D.P. Heinrichs, D.P. McNabb, H. Derrien, M.E. Dunn, N.M. Larson, L.C. Leal, A.D. Carlson, R.C. Block, J.B. Briggs, E.T. Cheng, H.C. Huria, M.L. Zerkle, K.S. Kozier, A. Courcelle, V. Pronyaev, S.C. van der Marck, Nuclear Data Sheets 107 (12) (2006) 2931.

[18] S.M. Dancoff, Physical Review 72 (1947) 1017.

[19] R. Serber, Physical Review 72 (1947) 1008.

[20] R.J. Glauber, Physical Review 99 (1955) 1515.

[21] J.R. Oppenheimer, Physical Review 47 (1935) 845.

[22] D. Ridikas, W. Mittig, J.A. Tostevin, Physical Review C 59 (1999) 1555.

[23] O.A. Shcherbakov, A.Y. Donets, A.V. Evdokimov, A.V. Fomichev, T. Fukahori, A. Hasegawa, A.B. Laptev, V.M. Maslov, G.A. Petrov, Y.V. Tuboltsev, A.S. Vorobiev, Journal of Nuclear Science and Technology Supplement 2 (1) (2002) 230.

[24] C. Paradela, L. Audouin, B. Berthier, I. Duran, L. Ferrant, S. Isaev, C. Lenaour, C. Stephan, L. Tassan-Got, D. Trubert, U. Abbondanno, G. Aerts, H. Alvarez, F. Alvarez-Velarde, S. Andriamonje, J. Andrzejewski, A. Angelopoulos, P. Assimakopoulos, G. Badurek, P. Baumann, F. Becvar, J. Benlliure, E. Berthoumieux, F. Calvino, D. Cano-Ott, R. Capote, A. CarrilloDeAlbornoz, P. Cennini, V. Chepel, E. Chiaveri, N. Colonna, G. Cortes, A. Couture, J. Cox, D. Cortina, S. Dababneh, S. David, R. Dolfini, C. Domingo-Pardo, I. Duran, C. Eleftheriadis, M. Embid-Segura, L. Ferrant, A. Ferrari, R. Ferreira-Marques, H. Frais-Koelbl,W. Furman, I. Goncalves, E. Gonzalez-Romero, A. Goverdovski, F. Gramegna, E. Griesmayer, F. Gunsing, B. Haas, R. Haight, M. Heil, A. Herrera- Martinez, K. Ioannides, S. Isaev, E. Jericha, Y. Kadi, F. Kaeppeler, D. Karamanis, M. Kerveno, V. Ketlerov, G. Kitis, P. Koehler, V. Konovalov, E. Kossionides, M. Krticka, C. Lamboudis, C. Leeb, A. Lindote, I. Lopes, M. Lozano, S. Lukic, J. Marganiec, L. Marques, S. Marrone, P. Mastinu, A. Mengoni, P. Milazzo, A. Molina, C. Moreau, M. Mosconi, F. Neves, H. Oberhummer, S. O'brien, J. Pancin, C. Papachristodoulou, A. Pavlik, P. Pavlopoulos, L. Perrot, R. Plag, A. Plompen, A. Plukis, A. Poch, C. Pretel, J. Quesada, W. Rapp, T. Rauscher, R. Reifarth, M. Rosetti, C. Rubbia, G. Rudolf, P. Rullhusen, J. Salgado, E. Savvidis, C. Stephan, G. Tagliente, J.L. Tain, L. Tavora, R. Terlizzi, N. Tsangas, G. Vannini, P. Vaz, A. Ventura, D. Villamarin, M.C. Vincente, V. Vlachoudis, R. Vlastou, F. Voss, M. Wendler, H. Wiescher, K. Wisshak, n-TOF fission data of interest to GEN-IV and ADS, in: PHYSOR-2006 Topical Meeting on Reactor Physics: Advances in Nuclear Analysis and Simulation, Vancouver, September 10–14, 2006, p. B076.

[25] A.V. Prokofiev, Nuclear Instruments and Methods in Physics Research Section A 463 (3) (2001) 557.

[26] F. Saint-Laurent, M. Conjeaud, R. Dayras, S. Harar, H. Oeschler, C. Volant, Nuclear Physics A 422 (1984) 307.

[27] J.T. Caldwell, E.J. Dowdy, B.L. Berman, R.A. Alvarez, P. Meyer, Physical Review C 21 (4) (1980) 1215.

[28] J.C. Sanabria, B.L. Berman, C. Cetina, P.L. Cole, G. Feldman, N.R. Kolb, R.E. Pywell, J.M. Vogt, V.G. Nedorezov, A.S. Sudov, G.Y. Kezerashvili, Physical Review C 61 (3) (2000) 034604.

[29] C. Cetina, P. Heimberg, B.L. Berman, W.J. Briscoe, G. Feldman, L.Y. Murphy, H. Crannell, A. Longhi, D.I. Sober, J.C. Sanabria, G.Y. Kezerashvili, Physical Review C 65 (4) (2002) 044622.

[30] H.A. Khan, R.J. Peterson, The International Journal of Radiation Applications and Instrumentation, Part D. Nuclear Tracks and Radiation Measurements 15 (1–4) (1988) 357.

[31] H.A. Khan, N.A. Khan, R.J. Peterson, Physical Review C 35 (2) (1987) 645.